mixture of DPPC and Bodipy-PC molecules under the influence of the electric field, resulting in the concentration gradient of Bodipy-PC in LE domains near the boundary of LC domains. Even though the monolayers were sampled only from compression cycles and were not compared with the samples from expansion cycles, we believe that the partition of fluorescent molecules had reached equilibrium at the moment of transfer. The interval between compression and transfer (several minutes) was enough time for the distribution of fluorescent molecules to reach equilibrium through diffusion. The diffusion coefficient of DPPC in the LE domain is 10^{-7} to 10^{-8} cm^2/s.

16. Averaged half-decay lengths (the lateral distances where the fluorescent intensities fall to half those of the maxima) determined from the cursor profiles across the domain boundaries for the monolayers sampled at π = 7, 10, 20, and 30 mN/m were 661 ± 133, 181 ± 38, 65 ± 15, and 37 ± 8 nm, respectively, in DPPC/Bodipy-PC samples and 345 ± 31, 143 ± 33, 57 ± 17, and 56 ± 13 nm, respectively, in the samples with an additional 0.5 mol % of ganglioside G_{M1}.
17. E. Betzig and R. J. Chichester, *Science* **262**, 1422 (1993).
18. The peak signal from a single lipophilic carbocyanine dye, dil-C_{18}(3) (Molecular Probes, D-282), molecule in a transferred DPPC monolayer was ~250 counts per second (cps) per nanowatt of tip power, which is ~20% of the typical value for a single molecule embedded in polymethylmethacrylate (*17*). This implies a quantum yield of ~0.2 for a Bodipy in the monolayer, resulting in the equivalent emission signal of 1200 cps/nW. In DPPC/Bodipy-PC samples, average intensities of the LE phase are ~35,000 cps/nW at π = 4 mN/m and ~75,000 cps/nW at π = 7 mN/m. The calculated number densities of the dye molecules in this phase are ~7.4×10^3 and ~1.3×10^4 molecules/μm^2, respectively.
19. J. Hwang, E. Betzig, M. Edidin, R. J. Chichester, *Biophys. J.* **66**, A277 (1994).
20. Dark spots at the center were caused by the dwell of the probe at one spot during the characterization of the near-field signal before scanning began.
21. We thank R. Chichester and R. Pagano for their valuable help and suggestions and H. McConnell for helpful discussions. Supported by NIH grants AI14584, DK44375 (M.E.), and AI30557 (L.K.T.).

8 June 1995; accepted 10 August 1995

Rapid Clay Mineral Formation in Amazon Delta Sediments: Reverse Weathering and Oceanic Elemental Cycles

Panagiotis Michalopoulos and Robert C. Aller*

Formation of aluminosilicate minerals in marine sediments was proposed over 30 years ago as a potentially important control on the chemistry of the oceans. Until now, this reverse weathering process has been largely discounted because of insufficient direct evidence for its existence. Experiments with unaltered, anoxic, Amazon delta sediments showed that substantial quantities of K-Fe-Mg clay minerals precipitated on naturally occurring solid substrates over times of ~12 to 36 months at ~28°C. A range of pore-water, solute-flux, and solid-phase criteria indicates that comparable clay mineral precipitation processes occur throughout Amazon shelf sediments, contributing ≥3 percent of the weight of the deposits and consuming ~10 percent of the global riverine K^+ flux.

The rapid formation of authigenic clay minerals during early sedimentary diagenesis was originally hypothesized as a likely process substantially influencing oceanic chemistry and closing a variety of elemental cycles through reverse weathering (*1*). The concept has not gained wide acceptance because of the lack of direct evidence for precipitation of such minerals in major deltas. Discovery of massive hydrothermal cycling of elements at midocean ridges has also decreased the obvious necessity for sedimentary sinks for certain solutes in geochemical budgets (*2*). However, problems concerning the geochemical balance of several major and minor elements still exist and can be overcome if early diagenetic formation of aluminosilicate minerals is assumed (*3*).

Authigenic glauconitic green clays form in small but concentrated amounts in continental shelf sands, upwelling areas, and sedimentary microenvironments, but such clays are usually considered relict, forming over thousands of years (*4*). Low-temperature authigenic smectites are also known to form from siliceous biogenic debris and metal oxides in local regions influenced by hydrothermal metal sources (*5*). Evidence for clay formation in nearshore depositional environments with high sediment accumulation rates has been indirect and has usually been inferred from observed trends in pore water solutes (K, F, Mg, and Al) or from small changes in solid-phase elemental compositions and operational leaches (*6–8*). In these latter cases, transported debris dominates accumulated material and makes documentation of disseminated authigenic clays difficult. In a few cases, direct evidence for nearshore early diagenetic clay formation (for example, the presence of nontronite, illite-smectite, and berthierine) has been found (*9*, *10*). The presence of authigenic clays documented to date in a range of environments therefore makes it certain that such minerals can form under the right conditions. The major questions that remain are whether the formation of such phases is rapid and whether it is geochemically significant.

As part of a general study of diagenetic processes in Amazon delta sediments, we investigated the potential formation of authigenic minerals during deposition (*11*). The Amazon River contributes ~6% of the total river particulates delivered annually to the oceans (*12*). Most of the Amazon river sediment is deposited on the adjacent continental shelf as a prograding delta. The suspended matter in the river is primarily of Andean origin (~82%) (*13*). The remainder is contributed by weathering in the Amazon drainage basin and consists of cation-poor (such as kaolinite and amorphous material) and cation-rich (such as smectite) aluminosilicate particles and of Si,Al,Fe oxides and oxyhydroxides as discrete particles and particle coatings (*10*, *14*). Upon entering the ocean, this material is mixed with reactive planktonic debris (organic carbon and SiO_2) and undergoes a variety of diagenetic changes, including extensive mobilization of Fe and Mn (*15*).

We simulated the conditions under which authigenic mineral precipitation must take place in a series of sediment incubation experiments that allowed ready separation of reaction products from the sedimentary matrix. To do this, we inserted small quantities (~0.5 g) of well-characterized solid substrates directly into otherwise unaltered Amazon delta sediments. Sediment was collected from the upper ~1 to 2 m of both inshore and offshore delta sites by means of box and kasten-type gravity corers. Except for possible diffusive exchange with overlying water or physical reworking by currents, material was subsequently maintained under conditions typical of burial in the delta. Substrates were (i) standard kaolinite, representative of the cation-poor aluminosilicate material that is one product of the tropical weathering regime of the Amazon basin; (ii) quartz sand grains, also a typical transported sediment component; (iii) FeOOH-coated quartz grains, representative of lateritic debris and commonly present in these sediments; and (iv) glass beads, simulating amorphous silica diatom frustrules, a biogenic product of photosynthesis in the water column that is deposited in Amazon delta sediments (*16*). Each substrate type was attached by a thin film of epoxy onto an acrylic slide, covered with a 0.4-μm nuclepore membrane filter and a nylon mesh outer screen, and inserted into the center of 250- to 1000-ml plastic bottles filled with natural Amazon delta sediment (wet and unaltered). Bottles were

Marine Sciences Research Center, State University of New York, Stony Brook, NY 11794–5000, USA.

*To whom correspondence should be addressed.

filled and sealed under N_2 and anoxically incubated in larger, sealed glass jars at 28°C for 12 to 36 months. The precipitation probe substrates were retrieved from the sediment under a N_2 atmosphere, washed with O_2-free filtered seawater, and briefly equilibrated with O_2-free distilled, deionized water in order to eliminate seawater salt precipitation during subsequent freeze-drying. Isolated substrates were stored under N_2 until further solid-phase analysis.

Under the scanning electron microscope (SEM), substrates (ii) and (iii) showed extensive precipitation of aluminosilicate material between substrate mineral grains as well as on both sides of the nuclepore filters. In the case of glass beads, precipitate formed predominantly on the filter membrane. Extensive dissolution of beads was found in all the experiments, and in many instances the glass had completely dissolved. The kaolinite grains were disintegrated but no enrichment in cations was evident from microprobe analysis. In the FeOOH-coated quartz substrates, we observed alteration of the external parts of the FeOOH coating to a Si-Al-Fe–rich phase with traces of other cations. This was probably the result of a reconstitution reaction similar to those documented in natural coated particles from the same area (*10*). Enrichment in P was also detected.

In the quartz grain and FeOOH-coated quartz grain substrates, the precipitate filled the space between the grains, forming a mesh constructed from 1- to 10-μm individual crystallites (Fig. 1A). The crystallites had a curved platy morphology (Fig. 1B) with extensive development of the *ab* plane. Transmission electron microscopy (TEM) observations showed that some of the platy crystals had a subeuhedral pseudohexagonal morphology (Fig. 2) (*17*). X-ray powder diffraction analysis (wavelength = 1.14857 Å, from a synchrotron source) of the precipitate indicated the presence of a 10.0 Å peak and a broad 7.16 Å peak. Higher order peaks are broad and are indicative of a disordered structure (*18*). Some alteration of the minerals due to dehydration during sample preparation (freeze-drying) is likely. Energy-dispersive system (EDS) analyses and single-crystal TEM-EDS spectra show Si, Al, Fe, K, and Mg as the predominant cations in most crystals. The Al, Fe, and K content varied substantially between individual crystals.

These observations indicate that the precipitates are clay minerals. We ascribe the 10.0 Å type to a dominant K-Fe–rich phase, which is consistent with a mica-type clay mineral. The 7.16 Å peaks probably belong to a less abundant Fe-rich, K-poor phase. We also conducted wave-dispersive system (WDS) electron microprobe analyses on precipitates. These analyses probably represent an average composition of a multicrystal assemblage rather than a single mineral crystal (*19*). Elemental analyses were converted to structural formulas with the assumption of a total anion charge of −44 typical of a mica-type clay mineral. The average structural formula is: $(K_{0.96}Na_{0.05})$-$(Al_{3.27}Fe^{+2}_{0.90}Mg_{0.39}Ti_{0.03})(Si_{6.47}Al_{1.53})$-$O_{20}(OH,F,Cl)_4$. We assume that most of the iron is present in the mineral structure in the form of Fe^{+2}, because the sediments are anoxic and are characterized by high concentrations of dissolved Fe^{+2}, a typical property of Amazon shelf sediments (*15*, *20*). Traces of Ca and Mn were also detected. NH_4^+, which is abundant in the pore waters, is probably also present in the clay but was not measured. Comparison with reported chemical compositions of other Fe-rich, K-rich, mica-type clay minerals such as glauconite (*21*) shows that the precipitates are depleted in Fe and enriched in Al.

The incubation experiments directly demonstrate the potential for rapid precipitation of clay minerals in Amazon delta sediments and indicate their likely structure and average composition (*22*). A variety of additional field evidence suggests that substantial disseminated authigenic clay that is consistent with the experimentally observed composition does indeed form. Pore water profiles in Amazon delta topset beds show depletion of F^- and K^+ with depth, despite rapid physical reworking of the upper ~1 to 2 m of the seafloor (*8*). On the basis of pore water transport models, direct measures of reaction rates, and operational solid-phase leaches, Rude and Aller estimated that ~7% of the riverine F^- supply to the oceans is taken up on the Amazon shelf and that formation or reconstitution of clay minerals is the most probable cause of both F^- and K^+ uptake (*8*). Estimated F/K flux ratios were in the general range expected for the occurrence of clay mineral precipitation.

The compositions of aluminosilicate material that we observed on the precipitation probes agree with these previous inferences. The F^- content of the experimental precipitates is in the range of 0.0146 to 0.3056 mole percent (mol%), with an average value of 0.148 mol%. The potassium content of the precipitates ranges from 3.9 to 11.0 mol%, with an average value of 6.98 mol%. Compared with other K-rich clays (transported illites), the neoformed clays are depleted in K. This apparent depletion could be the result of the presence of a K-poor phase that might have contaminated the analysis or could result from the presence of a mixed-layer clay mineral. Alternatively, it can be explained by a process similar to but more rapid than the one proposed by Odin and Matter for the neoformation of glauconite (*21*). They proposed that the first material precipitating from solution is poorly crystallized, K-poor, and Fe-rich with a high layer charge and that the precipitate evolves with time to a better crystallized K-enriched phase.

Simple mass balance calculations from the available fluorine flux data and the chemical composition of the precipitates indicate that neoformation of K-rich clay minerals in the Amazon delta has implications for the global K and F budgets. The

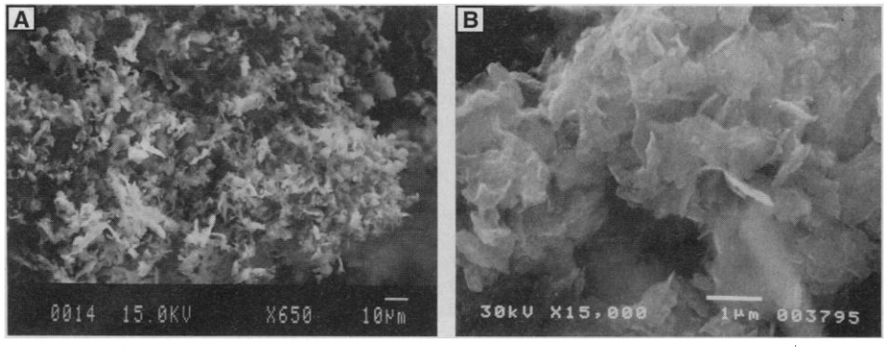

Fig. 1. (**A**) SEM picture of three-dimensional mesh precipitate of authigenic clay, formed between quartz sand substrates after ~18 months of incubation (scale bar, 10 μm). (**B**) SEM picture of authigenic clay crystallites demonstrating apparent monomorphological character with a curved flake shape (scale bar, 1 μm). The average structural formula given in the text was derived from microprobe analyses of comparable multiple crystals.

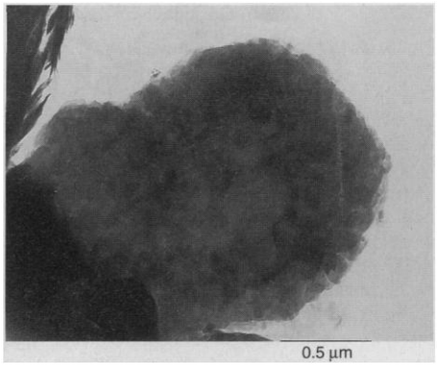

Fig. 2. Bright-field TEM image of Fe-rich precipitate. The crystallite exhibits a pseudohexagonal morphology and is composed of smaller pseudohexagonal crystals (scale bar, 0.5 μm).

flux of fluorine into the sediments predicted from pore water profiles (nonsteady-state minimum) ranges from 28 to 268 mmol m^{-2} day^{-1}. The estimated average annual fluorine sink in these sediments, calculated solely from aerially weighted pore water profile fluxes, is 2.6×10^9 mol $year^{-1}$ (*23*). The average F/K ratio measured on the neoformed clays is 21 mmol mol^{-1}, with a range of 4.4 to 41.37 mmol mol^{-1}. If this average compositional ratio holds for authigenic precipitates on the shelf, the annual K sink in Amazon continental shelf sediments amounts to 4.8×10^{12} g, representing ~10% of the annual riverine K supply to the oceans (*24*). This process of K uptake likely occurs in other depositional environments. Tropical river systems in general deliver ~60% of the continental particle flux to the oceans, and their muddy deltas may have similar diagenetic characteristics to that of the Amazon. Thus, the formation of K-rich clays in shelf environments with high sediment supply combined with processes of K uptake during low-temperature alteration of the upper oceanic crust (*25*) may contribute substantially to balancing the global budget of potassium.

Clay mineral formation and FeOOH coating alteration reactions require sources of both Al and Si. The incubation experiments demonstrate that Al must readily migrate in solution in order to pass the precipitation probe membranes. The source of Al must be the dissolution of relatively unstable amorphous Al oxides or other highly weathered aluminosilicate material (*26*). Because there is no evidence for unusually high concentrations of dissolved Al in Amazon delta sediments, there must be a close coupling of dissolution and reprecipitation reactions without buildup of dissolved Al intermediates. It is clear, however, that although Al may not migrate large distances, a portion is reactive. The common apparent immobility of Al does not preclude its involvement in near-simultaneous dissolution-precipitation processes.

There are a number of indications that the major limitation on authigenic clay mineral formation in Amazon delta sediments is likely to be the supply of reactive silica. The dissolution of glass beads in the precipitation experiments suggests that clay mineral precipitation results in substantial undersaturation of pore waters with respect to amorphous silica. Measured levels of dissolved silica in Amazon shelf pore waters are typically $\lesssim$200 μM over the upper ~1 m and often reach only ~300 μM at depths up to ~8 m, which are some of the lowest concentrations reported from marine sediments and are substantially below opaline silica solubility (Fig. 3A). In addition, diffusive fluxes of dissolved silica across the sediment-water interface are among the lowest ever measured in shallow marine environments and often show uptake from the water column, particularly in regions underlying turbid inshore waters of low productivity that are away from the dominant offshore sources of diatom debris (Fig. 3B). Although there is a large flux of diatomaceous debris to the bottom, little is preserved or buried as such (*27*). At least a portion of the solid biogenic silica flux may be converted into authigenic clay. The proposed control of biogenic silica over the amount of authigenic clays formed has implications for the geochemical budget of silica. If such control is confirmed in the future, it would result in the addition of authigenic clay formation to the known list of biogenic silica sinks in the oceans (*28*).

The pH of Amazon sediment pore waters is in the typical range of ~7.2 to 7.4 and is not particularly corrosive to siliceous debris. One possible mechanism for Si mobilization in the incubations and under field conditions comes from the known coupling of Fe redox cycling with Si (from quartz and diatom frustules) dissolution (*29*). This coupled mechanism is particularly viable in Amazon shelf sediments, where Fe cycling during organic matter remineralization dominates early diagenetic properties, and the extensive physical reworking of sediments causes repetitive redox oscillations, regenerating FeOOH. The dissolution-precipitation process, balanced for the stoichiometry of the neoformed clay minerals in Amazon delta sediments, is shown in Fig. 4.

As the Si, Al, and Fe reactant sources are essentially highly degraded weathering products, the general schematic reaction may be viewed as a form of reverse weathering. Reconstitution reactions of less degraded weathering products almost certainly also occur. These reactions likely result in dissemi-

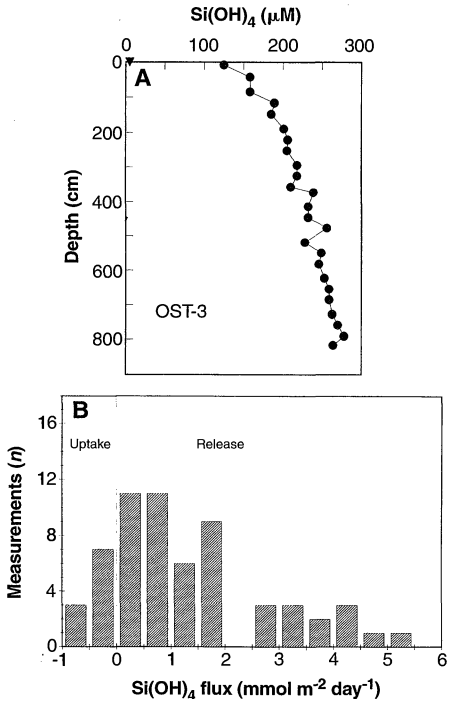

Fig. 3. (**A**) Representative pore water concentration profile of dissolved $Si(OH)_4$ in a piston core from station 4213, Open Shelf Transect 3 (OST-3), obtained from the high-accumulation-rate region of the Amazon delta topset deposits. Concentrations are typically 100 to 200 μM in the upper ~1 to 2 m of sediment over much of the delta topset region and tend to be ~300 μM at depth.The water column value (~5 μM) close to the sediment-water interface is shown by a solid triangle. (**B**) Frequency histogram of net diffusive fluxes of dissolved $Si(OH)_4$ across the sediment-water interface obtained by incubation cores (24 hours) at eight stations. Stations were sampled seasonally at four different times. Inshore stations often show net uptake of $Si(OH)_4$ from overlying water despite the absence of benthic photosynthesis. The mean annual flux from the delta deposits is ~1.3 mmol m^{-2} day^{-1}.

Release of reactants to solution (1)

$$6.47SiO_2 + 4.8Al(OH)_3 + 0.9Fe(OH)_3 + 0.225C_{org} + 3HCO_3^- + 12.49H_2O \rightarrow 6.47Si(OH)_4 + 4.8Al(OH)_4^- + 0.9Fe^{+2} + 3.225CO_2$$

Clay mineral neoformation (2)

$$6.47Si(OH)_4 + 4.8Al(OH)_4^- + 0.9Fe^{+2} + 0.96K^+ + 0.39Mg^{+2} + 0.05Na^+ + 0.03Ti(OH)_4 + 1.19CO_2 \rightarrow (K_{0.96}Na_{0.05})(Al_{3.27}Fe^{+2}_{0.90}Mg_{0.39}Ti_{0.03})(Si_{6.47}Al_{1.53})O_{20}(OH)_4 + 1.19HCO_3^- + 20.01H_2O$$

Net reaction (3)

$$6.47SiO_2 + 4.8Al(OH)_3 + 0.9Fe(OH)_3 + 0.225C_{org} + 0.96K^+ + 0.39Mg^{+2} + 0.05Na^+ + 0.03Ti(OH)_4 + 1.81HCO_3^- \rightarrow (K_{0.96}Na_{0.05})(Al_{3.27}Fe^{+2}_{0.90}Mg_{0.39}Ti_{0.03})(Si_{6.47}Al_{1.53})O_{20}(OH)_4 + 2.035CO_2 + 7.52H_2O$$

Fig. 4. Likely schematic reactions that lead to the neoformation of clay minerals. SiO_2 derives from skeletal material or other sources (such as quartz dissolution during redox oscillation); $Al(OH)_3$ comes from Al-oxide dissolution. Aluminosilicate dissolution is another potential source of Al and Si. Even though dissolution of an aluminum phase was not directly observed in our experiments, previous studies from the same region have demonstrated that such a process occurs (*6*). Fe^{+2} is from Fe reduction coupled with organic matter oxidation; K, Na, and Mg come from seawater; and Ti comes from dissolution of a Ti-bearing solid phase. Comparable reaction schemes for the formation of authigenic nontronite and illite-smectite have been proposed for sediments in Kaneohe Bay, Hawaii (*9*). In this case, Mg, Ca, and (to a lesser extent) Na and K showed depletions in pore water profiles and were present in the inferred authigenic aluminosilicate phases. The aluminosilicate phases reacting were derived from basalt weathering on land.

nated authigenic clay minerals in a substantial proportion of highly weathered continental debris and have important implications for global controls of elemental cycling.

REFERENCES AND NOTES

1. F. T. Mackenzie and R. M. Garrels, *Am. J. Sci.* **264**, 507 (1966).
2. J. M. Edmond *et al.*, *Earth Planet. Sci. Lett.* **46**, 1 (1979).
3. R. Wollast and F. T. Mackenzie, in *Silicon Geochemistry and Biogeochemistry*, S. R. Aston, Ed. (Academic Press, San Diego, CA, 1983), pp. 39–76; F. T. Mackenzie, in *Encyclopedia of Earth System Science*, W. A. Nierenberg, Ed. (Academic Press, San Diego, CA, 1992), pp. 431–445.
4. G. S. Odin and P. D. Fullagar, in *Green Marine Clays*, G. S. Odin, Ed. (Elsevier, Netherlands, 1988), pp. 295–332.
5. G. M. McMurthy and H.-W. Yeh, *Chem. Geol.* **32**, 189 (1981); T. G. Cole, *Geochim. Cosmochim. Acta* **49**, 221 (1985).
6. J. E. Mackin and R. C. Aller, *Cont. Shelf Res.* **6**, 245 (1986).
7. ———, *Geochim. Cosmochim. Acta* **48**, 281 (1984).
8. P. D. Rude and R. C. Aller, *Cont. Shelf Res.* **14**, 883 (1994).
9. B. L. Ristvet, thesis, Northwestern University, Evanston, IL (1978); F. T. Mackenzie, B. L. Ristvet, D. C. Thorstenson, A. Lerman, R. H. Leeper, in *River Inputs to the Ocean*, J. M. Martin, J. D. Burton, D. Eisma, Eds. (United Nations Environment Programme– United Nations Educational, Scientific, and Cultural Organization, Geneva, Switzerland, 1981), pp. 152–187.
10. P. D. Rude and R. C. Aller, *J. Sediment. Petrol.* **59**, 704 (1989).
11. This project was part of A Multidisciplinary Amazon Sediment Study (AMASEDS) [see C. A. Nittrouer, D. J. DeMaster, Á. G. Figuereido, J. M. Rine, *Oceanography* **4**, 3 (1991)].
12. J. D. Milliman and J. P. M. Syvitski, *J. Geol.* **100**, 525 (1992).
13. R. J. Gibbs, *Geol. Soc. Am. Bull.* **78**, 1203 (1967).
14. K. O. Konhauser, W. S. Fyfe, B. I. Kroeberg, *Chem. Geol.* **111**, 155 (1994).
15. R. C. Aller, J. E. Mackin, R. T. Cox Jr., *Cont. Shelf Res.* **6**, 263 (1986); R. C. Aller, N. E. Blair, Q. Xia, P. D. Rude, *ibid.*, in press.
16. Substrate (i) was Ward's kaolinite standard no. 9, collected from Mesa Alta, NM. Substrate (ii) was quartz sand, grain size 200 to 400 μm. Substrate (iii) was quartz sand grains coated with a FeOOH-gel made from $FeCl_3$ and NaOH at a pH of 5. The resulting coating was x-ray amorphous, and the probable compound was FeOOH. For substrate (iv), the beads were made out of glass composed mostly of Si and containing some Ca, Na, and Mg. Size range was 20 to 60 μm.
17. Submicron crystallites composed of Si, Al, K, Fe, and Mg and having a curved morphology were ubiquitous under the TEM.
18. We did not analyze lattice spacings (d) larger than 10.2 Å. Because of the small amount of material available for x-ray diffraction analysis, we used a capillary tube sample holder and a synchrotron radiation source at Brookhaven National Laboratory. The wavelength used in conjuction with the geometry of the sample holder–detector setup did not allow data acquisition at low angles. Powder diffraction patterns also showed the presence of amorphous material.
19. It is possible that the presence of any K-poor phase might have contaminated the analyses of the K-Fe–rich phase. We also cannot exclude the possibility of mixed layering. In addition, it is difficult to assess the contribution from the amorphous material present in the precipitates. More than 90% of the analyses were dominated by the inferred K-Fe phase.
20. The pH of the sediments after the termination of the experiments was within the range of the in situ values measured during collection (7.2 to 7.4). Analysis of the pore waters after the termination of the experiments showed that Mg, Ca, Si, Fe, and total CO_2 concentrations were in the range measured in shelf pore waters.
21. G. S. Odin and A. Matter, *Sedimentology* **28**, 611 (1981).
22. Low-temperature (3° to 22°C) formation of clay minerals has also been observed under a variety of artificial laboratory conditions [H. Harder, *Chem. Geol.* **18**, 169 (1976); *Clays Clay Miner.* **26**, 65 (1978); *ibid.* **28**, 217 (1980)].
23. This value is approximately 25% lower than previously estimated in (*7*), based on a combination of pore water gradient data and reaction rate measurements.
24. E. K. Berner and R. A. Berner, *The Global Water Cycle: Geochemistry and Environment* (Prentice-Hall, Englewood Cliffs, NJ, 1987), chap. 8.
25. A. J. Spivack and H. Staudigel, *Chem. Geol.* **115**, 239 (1994).
26. A. C. Aplin, in *Geochemistry of Clay-Pore Fluid Interactions*, D. A. C. Manning, P. L. Hall, C. R. Hughes, Eds. (Chapman and Hall, London, 1993), pp. 81–106; J. E. Mackin and R. C. Aller, *Crit. Rev. Aquat. Sci.* **1**, 537 (1989).
27. D. J. DeMaster, G. B. Knapp, C. A. Nittrouer, *Geochim. Cosmochim. Acta* **47**, 1713 (1983); D. J. DeMaster, W. O. Smith Jr., D. M. Nelson, J. Y. Aller, *Cont. Shelf Res.*, in press.
28. P. Tréguer *et al.*, *Science* **268**, 375 (1995).
29. R. C. Morris and A. B. Fletcher, *Nature* **330**, 558 (1987); L. M. Mayer, J. Jorgensen, D. Schnitker, *Mar. Geol.* **99**, 263 (1991).

30. We thank R. Reeder for obtaining the TEM data, M. Kunz and J. Parise for obtaining the synchrotron powder diffraction data, and G. Symmes for assisting with the microprobe analyses. P. Rude, M. Green, and J. Mackin helped with the probe construction and experimental setup. P. Bartholomew assisted with SEM-EDS analyses. The participants of AMASEDS assisted in all aspects of the field work. Financial support was provided by NSF (R.C.A). A fellowship from the State Scholarship Foundation of Greece to P.M. is acknowledged.

27 April 1995; accepted 31 July 1995

Limits to Relief

Kevin M. Schmidt* and David R. Montgomery

Comparison of slope profiles in areas exhibiting widespread bedrock landsliding with the use of a model for the maximum size of stable hillslopes established that mountain-scale material strength can limit topographic relief. Conventional laboratory values for intact rock greatly exceeded integrative rock strength properties that were back-calculated from the upper limit to hillslope relief and gradient in the northern Cascade Range and Santa Cruz Mountains. Back-calculated strength values, however, were indistinguishable from those obtained through field and conventional laboratory measurements on the weakest members of each rock formation, as well as on glacial sediments along the Cascade front. These results contrast with the conventional assumption that relief is incision-limited and indicate that the relief of mountain ranges can reflect landscape-scale material strength, as well as the interaction of tectonic and climatic processes.

Relief is a fundamental landscape attribute that is widely recognized as reflecting the interplay of uplift and erosion (*1*). The role of material properties in relief development, however, is poorly understood. The conventional view that the relief of natural landscapes is incision-limited (*2*) reflects the observation that hillslope stability analyses using intact rock strengths predict the stability of cliffs kilometers in height (*3*). However, rock mass strength decreases with increasing spatial scale, because of the influence of spatially distributed discontinuities (*4*), and it has been unclear whether mountain-scale rock strength might be low enough to limit relief in bedrock landscapes (*1*). Through a regional field test of a slope stability model, we demonstrate here that mountain-scale material strength can limit relief development in bedrock landscapes.

A model for bedrock landsliding provides a framework for prediction of the maximum size of stable hillslopes or mountain fronts and thereby for the evaluation of the influence of material properties on relief development (*5*). As hillslope relief (H) increases, topographically induced gravitational shear stress across potential failure surfaces increases until it exceeds material strength and landsliding ensues. Culmann's two-dimensional, limit-equilibrium, slope stability model (*6*), which has been widely applied to unconsolidated deposits (*7*), predicts a bounding relation between hillslope gradient (β) and relief such that the maximum hillslope height (H_c) is given by

$$H_c = \frac{4c}{\gamma} \frac{\sin\beta \cos\phi}{[1 - \cos(\beta - \phi)]} \quad (1)$$

where c is cohesion, γ is unit weight, and ϕ is the internal friction angle. Hoek and Bray (*8*) modified Eq. 1 to incorporate pore water pressure, and Schmidt (*9*) integrated seismic accelerations. Assigning a representative γ, we used Eq. 1 to calculate landscape-scale c and ϕ from the upper limit to the range of β and H within a landscape. The actual material properties of incision-limited landscapes will exceed back-calculated values of c and ϕ, which indicates that bedrock strength could support deeper val-

Department of Geological Sciences, University of Washington, Seattle, WA 98195, USA.

*To whom correspondence should be addressed.